Optimization of the effective light attenuation length of YAP:Ce and LYSO:Ce crystals for a novel geometrical PET concept

I. Vilardi[a], A. Braem[b], E. Chesi[b], F. Ciocia[a], N. Colonna[a], F. Corsi[c], F. Cusanno[d], R. De Leo[a,*], A. Dragone[c], F. Garibaldi[d], C. Joram[b], L. Lagamba[a], S. Marrone[a], E. Nappi[a], J. Séguinot[b], G. Tagliente[a], A. Valentini[a], P. Weilhammer[b], H. Zaidi[e]

[a]Physics Department and INFN Section of Bari, Via Orabona 4, Bari, Italy
[b]CERN PH-Department, CH-1211 Geneva, Switzerland
[c]DEE Politecnico di Bari—MICROLABEN s.r.l., Bari, Italy
[d]Laboratory of Physics, ISS, Viale Regina Elena 299, Rome, Italy
[e]Division of Nuclear Medicine, Geneva University Hospital, CH-1211 Geneva, Switzerland

Abstract

The effective light attenuation length in thin bars of polished YAP:Ce and LYSO:Ce scintillators with lengths of the order of 10 cm has been studied for various wrappings and coatings of the crystal lateral surfaces. This physical parameter plays a key role in a novel 3D PET concept based on axial arrays of long scintillator bars read out at both ends by Hybrid Photodetectors (HPDs) since it influences the spatial, energy and time resolutions of such a device. In this paper we show that the effective light attenuation length of polished crystals can be reduced by wrapping their lateral surfaces with Teflon, or tuned to the desired value by depositing a coating of Cr or Au of well-defined thickness. The studies have been carried out with YAP and LYSO long scintillator bars, read out by standard photomultiplier tubes. Even if the novel PET device will use different scintillators and HPD readout, the results described here prove the feasibility of an important aspect of the concept and provide hints on the potential capabilities of the device.
© 2006 Elsevier B.V. All rights reserved.

1. Introduction

The CIMA collaboration [1] has proposed a novel 3D PET geometrical concept [2] based on axially oriented arrays of long polished scintillator bars (e.g. $3.2 \times 3.2 \times 100 \, mm^3$), read out at the two ends by Hybrid Photodetectors (HPDs) [3]. A schematic view of the novel device is shown in Fig. 1. The unambiguous definition of the γ-ray interaction point in a real 3D geometry eliminates [4] the parallax error due to the unknown depth of interaction (DoI) of the γ-ray thus improving the spatial resolution, sensitivity and contrast of the PET performance in the field of molecular imaging. The concept is new compared to available PETs which are based [2] on radial crystal arrangements and block readout schemes (Anger logic) [5]. It is conceptually different from the phoswich technique [5,6] which also aims to measure the DoI. The 3D Axial PET concept provides higher efficiency, due to the absence of limitations imposed by the detector thickness in the radial direction, and to the possibility [4] to recover a fraction of γ's undergoing double interactions (first Compton and then photoelectric in a different crystal of the same array).

*Corresponding author. Tel.: +39 080 5443242; fax: +39 080 5534938.
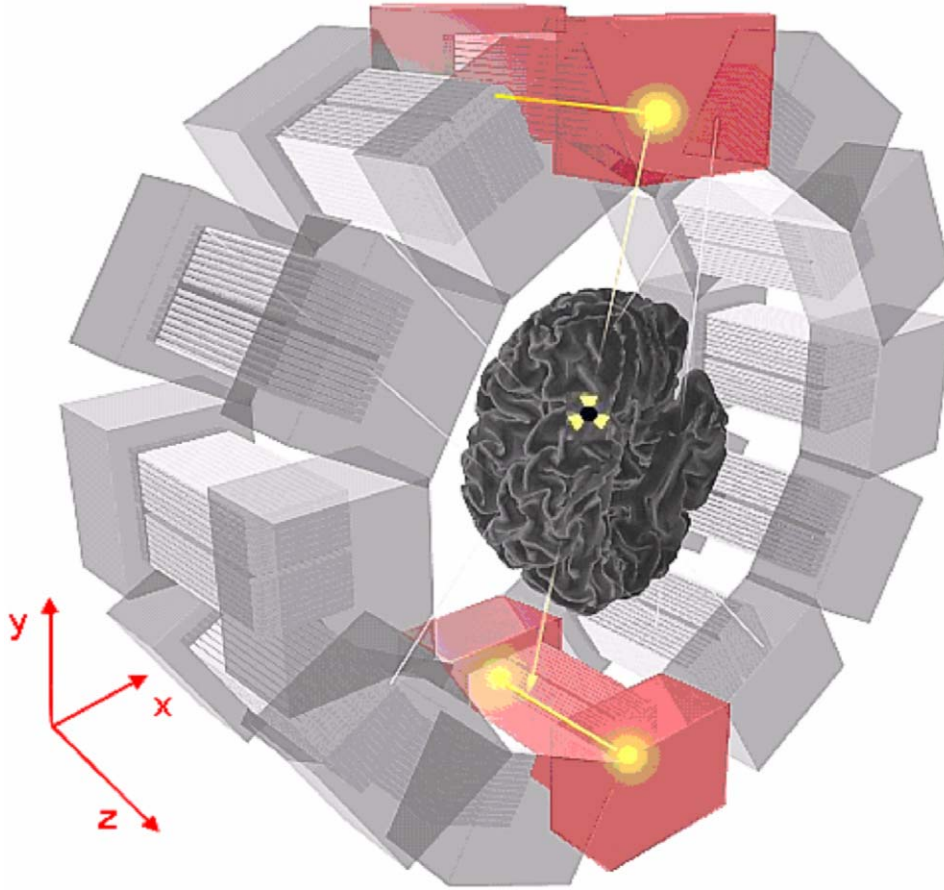E-mail address: deleo@ba.infn.it (R. De Leo).

Fig. 1. Schematic illustration of the 3D axial HPD-PET concept. Arrays of axially arranged long crystals are read out on both sides by HPDs.

Scintillation light produced in the crystal propagates to the two bar ends by internal reflection from the crystal lateral surfaces. On its way to the photodetectors, part of the light is absorbed with a characteristic attenuation length. While the transverse coordinates (x,y) of the detected γ-ray are determined from the address (i.e. position) of the hit crystal, deduced by both photodetectors with a spatial resolution [2] $\sigma_{x,y} = 3.2/\sqrt{12} = 0.92\,\text{mm}$, the axial ($z$) coordinate is derived with a precision σ_z from the ratio of the photoelectron yield, N_1 and N_2, measured at the two ends of the long crystals:

$$z = \frac{1}{2}\left(\lambda_{\text{eff}} \ln \frac{N_1}{N_2} + L_C\right),$$

$$\sigma_z = \frac{\lambda_{\text{eff}}}{\sqrt{2N_0}}\left(\exp\frac{z}{\lambda_{\text{eff}}} + \exp\frac{L_C - z}{\lambda_{\text{eff}}}\right)^{1/2}, \qquad (1)$$

with L_C being the length of the crystal. λ_{eff} is the effective light attenuation length and is different from the bulk value λ_{bulk} as it takes into account the real path of the photons, which is increased because of the multiple bounces: $\lambda_{\text{eff}} \approx 0.8\lambda_{\text{bulk}}$. The expression for σ_z accounts for the photoelectron statistics; however it ignores the fluctuations of the path lengths w.r.t. the average value. N_0 is the number of photoelectrons for $\lambda_{\text{eff}} \to \infty$. Its value depends

both on the physical and optical properties of the chosen scintillator (including surface coating/wrapping) and the characteristics of the photodetector. It is implicitly assumed that the photoelectron yields N_1 and N_2 depend exponentially on the average path length of the scintillation photons belonging to one γ-ray:

$$N_1 = \frac{N_0}{2}\exp\left(\frac{-z}{\lambda_{\text{eff}}}\right), \quad N_2 = \frac{N_0}{2}\exp\left(\frac{-(L_C - z)}{\lambda_{\text{eff}}}\right), \qquad (2)$$

giving the total number of photoelectrons N_{pe}:

$$N_{\text{pe}}(z) = N_1 + N_2. \qquad (3)$$

The statistical term of the energy and time resolutions can be expressed as:

$$\frac{\sigma_E}{E} = \sqrt{\frac{\text{ENF}}{N_{\text{pe}}}}, \quad \sigma_T = \frac{c}{\sqrt{N_{\text{pe}}}}, \qquad (4)$$

where ENF is the excess noise factor [7] of the photodetector and c is a constant. From the previous equations it can be seen that while an increase of N_0 improves all the resolutions, an increase of λ_{eff}, although improving σ_E/E and σ_T, worsens σ_z.

In order to achieve a competitive σ_z, the crystal length L_C needs to be limited to values below $\sim150\,\text{mm}$ and λ_{eff}

has to be optimized depending on the chosen scintillator and crystal length. The two parameters L_C and λ_{eff} play obviously a key role in the proposed geometrical PET concept.

In this paper we present an experimental study to optimize the effective light attenuation length, λ_{eff}, for a set of polished YAP:Ce scintillators of dimensions $3.2 \times 3.2 \times 100\,mm^3$ produced by Preciosa Crytur Co. at Turnov, Czech Republic, and for a few samples of polished LYSO:Ce of equal size, produced by Photonic Materials, Bellshill, Scotland. We have measured the λ_{eff} parameter in polished and wrapped crystals by means of 511 keV γ-rays emitted from an ^{22}Na source.

Techniques to modify the reflectivity of the crystal by wrapping, coating and, mostly, roughing its surface have been described [8] in the literature. We show here that, by coating the lateral surfaces of the polished crystals with layers of evaporated Cu or Au of various thicknesses, it is possible to tune λ_{eff} to achieve a value which leads to optimized spatial, energy and time resolutions.

A simulation with the photo tracking code Litrani [9] has been used to extrapolate the present study to other crystal coatings. The code will be used to predict results for other crystal lengths and for other scintillators, such as LaBr$_3$ and LSO. The latter ones, having both high photofraction and light yield, appear hence more suited for PET devices. Experimental studies with these crystals are in progress.

Studies reported in the literature about PET designs [8,10–13] where the DoI information is obtained reading out both crystal ends [14], refer to conventional PET geometries with shorter scintillator bars (2–3 cm) and a surface finish different (raw) from ours, thus favouring diffuse reflection of scintillation light from the crystal lateral surfaces, rather than specular one.

2. Experimental set-up and results

2.1. Experimental apparatus

We have carried out the experimental studies with YAP and LYSO crystals of dimensions $3.2 \times 3.2 \times 100\,mm^3$. Their refractive indices (at the emission wavelength maximum) are $n_{LYSO} = 1.82$ (420 nm) and $n_{YAP} = 1.94$ for YAP (370 nm). The thickness of the crystal has been chosen to obtain an excellent transverse spatial resolution and is matched to the segmentation of the HPDs that will be used in the final project [2,3]. A set-up has been built (see Fig. 2), which allows measuring the effective attenuation lengths. The crystal under test is read out by two photodetectors and is placed on a linear stage remotely movable by a step motor.

For the present study two H3164-10 PMTs[1] with bialkali photocathodes and borosilicate windows ($n_{win} = 1.47$) have been used as photodetectors. The PMTs are coupled to the scintillator with optical grease (BC-630 from Bicron,
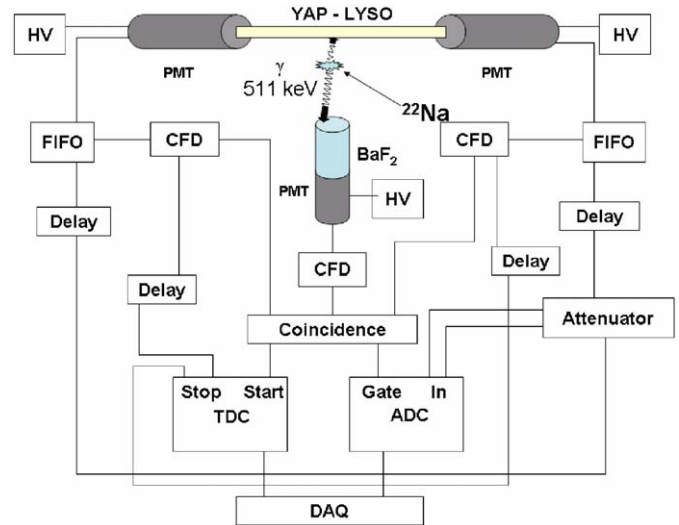

Fig. 2. Schematic set-up used to measure effective light attenuation lengths.

$n_{BC-630} = 1.47$). The HPDs of the final device will be equipped with a thin sapphire window ($n = 1.793$ at 370 nm, $n = 1.782$ at 420 nm), thus leading to an almost perfect refractive index matching which minimizes transmission losses at the crystal–detector interface. In this latter case, an optical coupling oil, like the one commercialized by Cargille–Sacher Laboratories, Inc. [15], with a refractive index higher than that of BC-630, will be used.

A point-like ^{22}Na source sealed in plastic has been used. One of the two resulting 511 keV γ-rays is detected by the crystal that is placed in coincidence with a cylindrical BaF$_2$ scintillator (2 cm diameter, 6 cm length) detecting the second 511 keV γ-ray. The BaF$_2$ detector and the γ-source are placed at a fixed position outside of the linear stage. The radioactive source is collimated with a 4 mm lead shield block with a rectangular opening. It is positioned 45 cm from the BaF$_2$ detector and 5 cm from the face of the tested YAP or LYSO crystal in order to illuminate a 2-mm-wide slide of its lateral surface. Conventional NIM electronics has been used. The data acquisition has been restricted to coincident timing signals from the crystal-left, crystal-right and BaF$_2$ PMTs. Timing signals have been formed by employing constant fraction discriminators (CFD). A scheme of the electronics used is included in Fig. 2.

An example of the obtained spectra (sum of the left and right signals) for polished YAP and LYSO crystals with 511 keV γ-rays impinging at the crystal centre ($z = 5\,cm$) is shown in Fig. 3. The LYSO scintillator has a higher photofraction and produces more photoelectrons than YAP, as a consequence of a higher photon yield [2] (27 ph/keV for LYSO, 18 ph/keV for YAP), of a lower refractive index and, as will be shown later, of a longer light attenuation length. But, in spite of the higher photoelectron number, the energy resolution of LYSO is worse than that of YAP, most probably due to a higher intrinsic
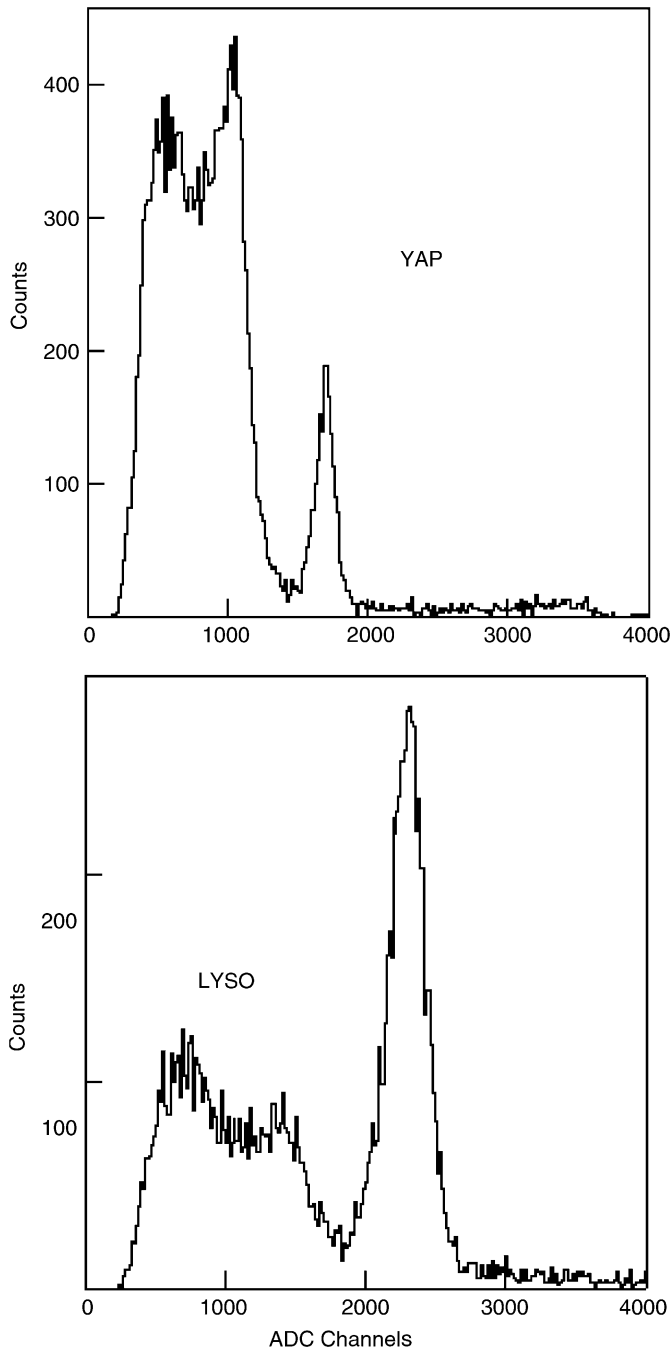
Fig. 3. Energy spectra for polished YAP (upper panel) and LYSO (lower panel) scintillators exposed to 511 keV γ-rays impinging at the centre of the crystal lateral surface. The spectra have been obtained by summing the crystal left and right ADC signals in coincidence with the BaF$_2$ signal. The shown spectra have been obtained with same high voltages for the left and for the right H3164-10 PMTs.

Fig. 4. Bidimensional spectrum (left versus right ADC channels) for a $3.2 \times 3.2 \times 100\,mm^3$ polished YAP crystal exposed to 511 keV γ-rays at the centre ($z = 5\,cm$) of its lateral surface. The spectrum has been taken in coincidence with a BaF$_2$ crystal detecting the second 511 keV γ-ray from an ^{22}Na source.

2.2. Measurement of the effective light attenuation length λ_{eff}

The signal amplitudes measured at left and right ends of the crystal bar are highly correlated. Fig. 4 illustrates this for a polished YAP scintillator exposed to 511 keV γ-rays impinging in the middle ($z = 5\,cm$) of the crystal bar. The central spot in the figure corresponds to the photopeak. In Fig. 5 we plot Q, the charge of the photopeak (in ADC counts), as obtained from the left ADC spectrum, scanning polished YAP and LYSO crystals in the z range from 1 to 9 cm, in steps of 1 cm. The linear behaviour in log scale means that one exponential ($Q_0 \exp[-z/\lambda_{eff}]$) is sufficient to describe the PMT pulse height as a function of the distance z of the γ-source from the PMT.

The average effective attenuation length evaluated on a set of 16 polished YAP crystals results to be $\lambda_{eff} = 20.8 \pm 0.4\,cm$. This value is higher than those reported in the literature [2,16] and, as we will discuss below, would lead to a worse resolution of our z-reconstruction method. For a set of three polished LYSO crystals an even higher value, $\lambda_{eff} = 42.0 \pm 0.9\,cm$, has been obtained. Also this value is higher than those (2–4 cm) that can be deduced from the data in Refs. [8,10–13] that however refer to LSO scintillators not mechanically polished.

In Fig. 6 we report the results of the same z scans for YAP crystal bars with the lateral surfaces coated or wrapped. The experimental data show that the behaviour of coated or wrapped crystals is also well reproduced by one exponential. The resulting light attenuation lengths λ_{eff} are reported in Table 1. The investigated wrappings/coatings result in λ_{eff} values in the range 3.9–11.9 cm, compared to 20.8 cm for the polished uncoated YAP crystal. Although each of the wrappings/coatings can effectively reduce λ_{eff}, only the Teflon wrapping is able to

resolution [2,16]. The $\Delta E/E$ (FWHM) values are: 10.8% for YAP and 14.6% for LYSO. This last value is comparable with those quoted in literature: 13–15% [10] and 14–18% [8], both obtained for 20-mm-long LSO raw bars. The YAP energy resolution is better than the 14% value quoted in Ref. [16] for 30 mm long bars.
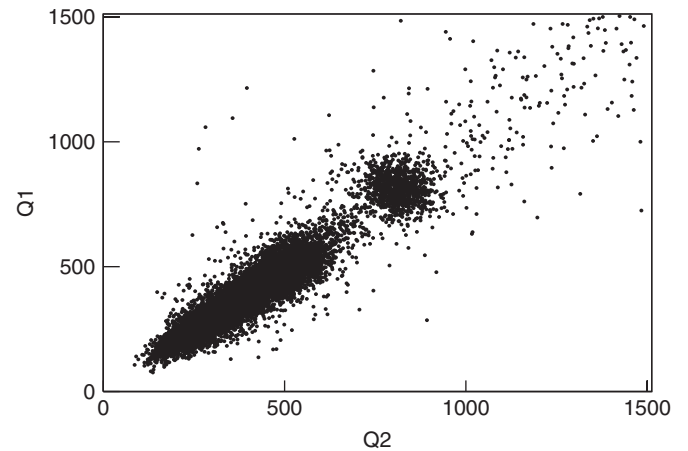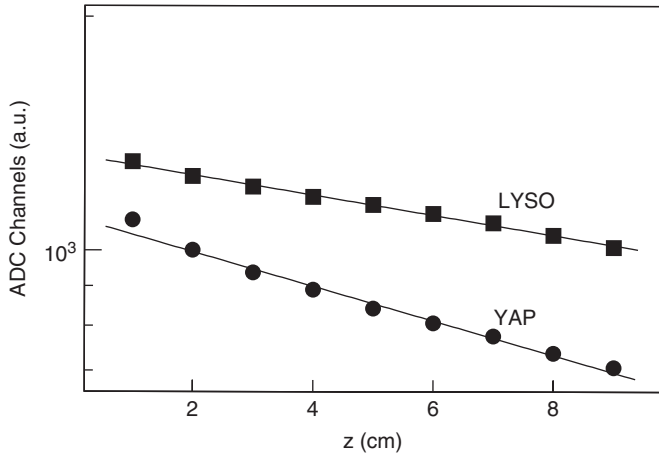
Fig. 5. The 511 keV γ-ray photopeak signal amplitude (log scale) measured at one end of the bar (here left) versus the z position of the [22]Na source on the lateral surface of a polished YAP and LYSO crystal. The different slope of the two sets of points is due to the different λ_{eff} value for the two scintillators.

Table 1
Measured λ_{eff} values and spatial, energy and time resolutions for 10-cm-long YAP and LYSO crystals with different coatings

	λ_{eff} (cm)	σ_E/E (%)	σ_z (mm)	σ_t (ps)
YAP polished	20.8 ± 0.4	4.6 ± 0.4	8.2 ± 0.3	440 ± 15
YAP Cr (1 nm)	11.9 ± 0.3	5.2 ± 0.3	7.1 ± 0.4	480 ± 15
YAP white painted	10.7 ± 0.2	6.2 ± 0.3	6.5 ± 0.2	550 ± 20
YAP Tefl. wrap.	10.5 ± 0.3	4.7 ± 0.2	5.4 ± 0.3	470 ± 20
YAP black painted	5.4 ± 0.2	10.6 ± 0.7	6.1 ± 0.3	775 ± 30
YAP Au (1.5 nm)	5.2 ± 0.2	7.7 ± 0.8	4.8 ± 0.4	640 ± 35
YAP Cr (3 nm)	3.9 ± 0.2	13.4 ± 1.5	5.3 ± 0.2	925 ± 30
LYSO polished	42.0 ± 0.9	6.2 ± 0.2	14.4 ± 0.4	420 ± 10
LYSO Tefl. wrap.	20.0 ± 0.5	7.0 ± 0.2	9.3 ± 0.3	490 ± 10

All measurements have been performed with γ-rays of 511 keV in the centre of the crystal.
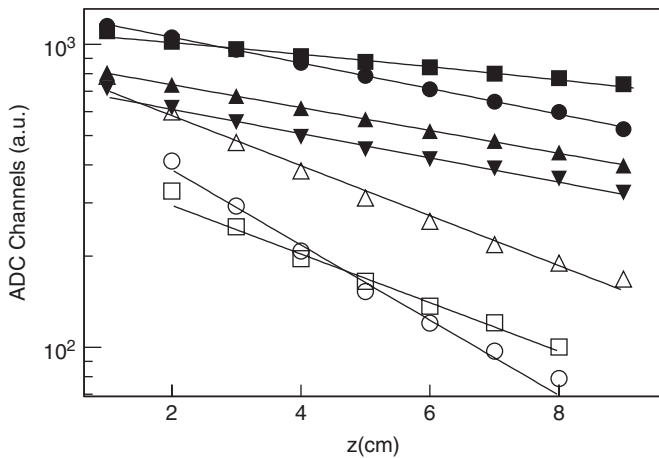All resolutions have been evaluated from the standard deviation of the photopeak of the sum spectra $N_1 + N_2$.
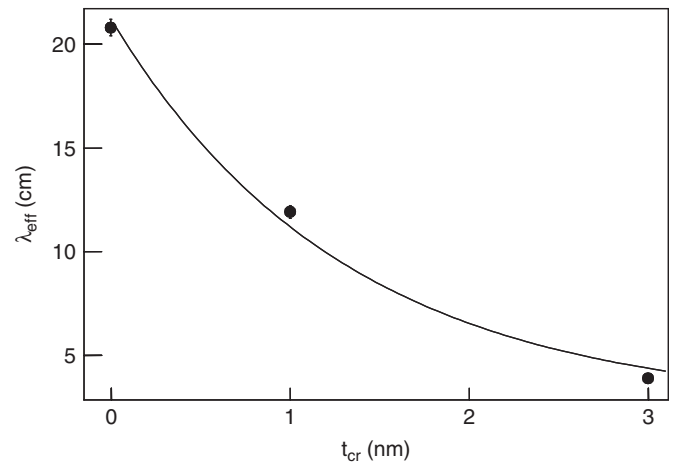

Fig. 6. Pulse height of the photopeak centroids as delivered by a H3164-10 PMT for 511 keV γ-rays impinging laterally on a 10-cm-long YAP crystal at different z positions. Full squares refer to a polished crystal, full points to a Teflon-wrapped crystal, upward full triangles to a crystal coated with 1 nm Cr, downward full triangles to a white painted crystal, upward empty triangles to a crystal coated with 1.5 nm Au, empty squares to a black painted crystal, empty circles to a crystal coated with 3 nm Cr. The lines on the experimental points are exponential fits to the data, giving the light attenuation lengths λ_{eff} reported in Table 1. The extrapolation of the fits to $z = 0$ gives a rough estimate of $N_0/2$ (see Eq. (1)). The N_0 parameter is obviously also affected by the surface properties of the crystal.

Fig. 7. Experimental λ_{eff} values (points) obtained for polished (point at $t_{Cr} = 0$ nm) and Cr-coated YAP crystals compared with the prediction (full line) of a photo tracking code [9].

practically halve it and to maintain, at the same time, a high light yield.

The metallic evaporation method has the advantage to allow tuning λ_{eff} to a desired value by changing the coating thickness. This is shown in Fig. 7 where the experimental λ_{eff} values obtained for Cr-coated and -polished YAP crystals are plotted and compared with the prediction of a photo tracking code [9], run with the following values: 24 cm for the YAP bulk attenuation length λ_{bulk}, 0.109 nm for the Cr absorption length $\lambda_{abs}(370\,nm)$ and 1.87 for the Cr refractive index $n_{Cr}(370\,nm)$.

The effectiveness of Teflon in reducing the photon attenuation length has also been proved for LYSO crystals. The effects of other wrappings/coatings have not been tested on LYSO because currently only few crystal samples are available. Presumably the effects are the same as for YAP.

We remark that the extrapolations of the data in Fig. 6 to $z = 0$ (which correspond to $N_0/2$) show that the light collection efficiency is strongly dependant on the wrapping/coating. Simulations are ongoing in order to reproduce this reduced detected light yield.

2.3. Reconstruction of the z coordinate

The reconstructed z coordinate of the γ-ray interaction point in the crystal is derived from the ratio of signals at the left and right bar ends using Eq. (1). Fig. 8 shows the mean value of the reconstructed z coordinate for photopeak events, plotted as a function of the true z coordinate.
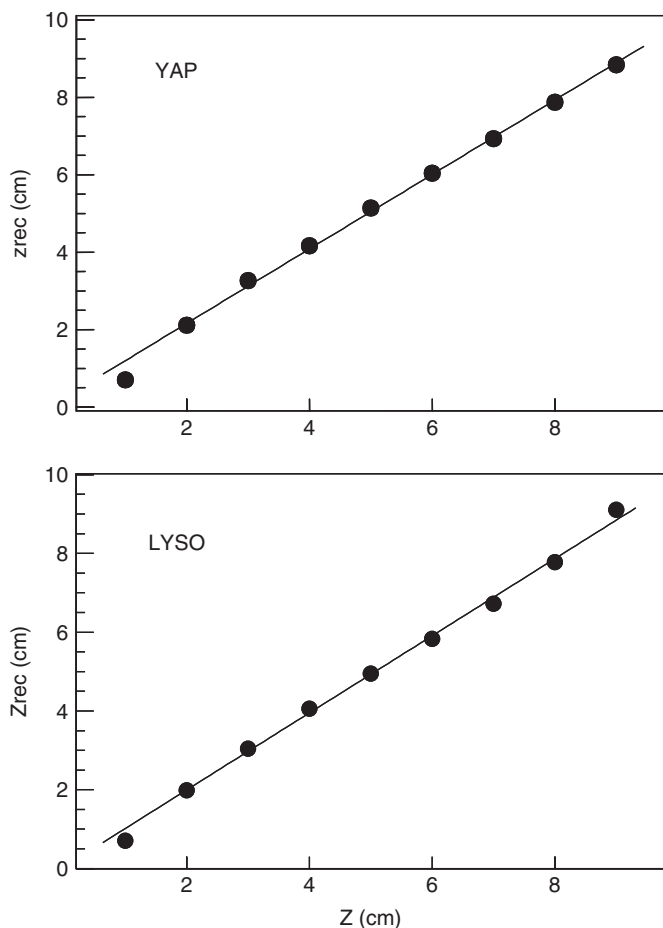
Fig. 8. Reconstructed z positions (points) versus the real ones, for a polished YAP (upper panel) and LYSO (lower panel) crystal. The reconstruction is restricted to photopeak events. The continuous lines are linear fits to the data.

Fig. 9. Distributions of the reconstructed z points for individual 511 keV γ-rays in a Teflon-wrapped YAP crystal at three distances $z = 2$, 5 and 8 cm for top, central and lower panel, respectively.

These measurements result from averaging over many events, such that the statistical error of the mean value becomes negligible (smaller than the marker size in the figure). The upper panel of the figure is for a polished uncoated YAP and the lower one for a LYSO crystal. The data are very well described by a linear fit, proving the validity of the applied reconstruction method. A small deviation from linearity is observed towards the bar ends. Similar results have been obtained for coated and wrapped crystals. The non-linearity at the ends is slightly enhanced for the shorter λ_{eff} values. The small discrepancy on the z-reconstruction at the bar end can be explained by the small increase of the solid angle in collecting the light.

The distributions of the reconstructed z points for individual 511 keV γ-rays are shown in Fig. 9 for a Teflon-wrapped YAP crystal for three different interaction depths ($z = 2$, 5 and 8 cm). These have a Gaussian shape whose standard deviations, giving the σ_z resolution in z-reconstruction, are shown in Fig. 10, both for YAP (left panels) and LYSO (right panels) crystals, in polished (upper panels) and Teflon-wrapped (lower panels) condi-
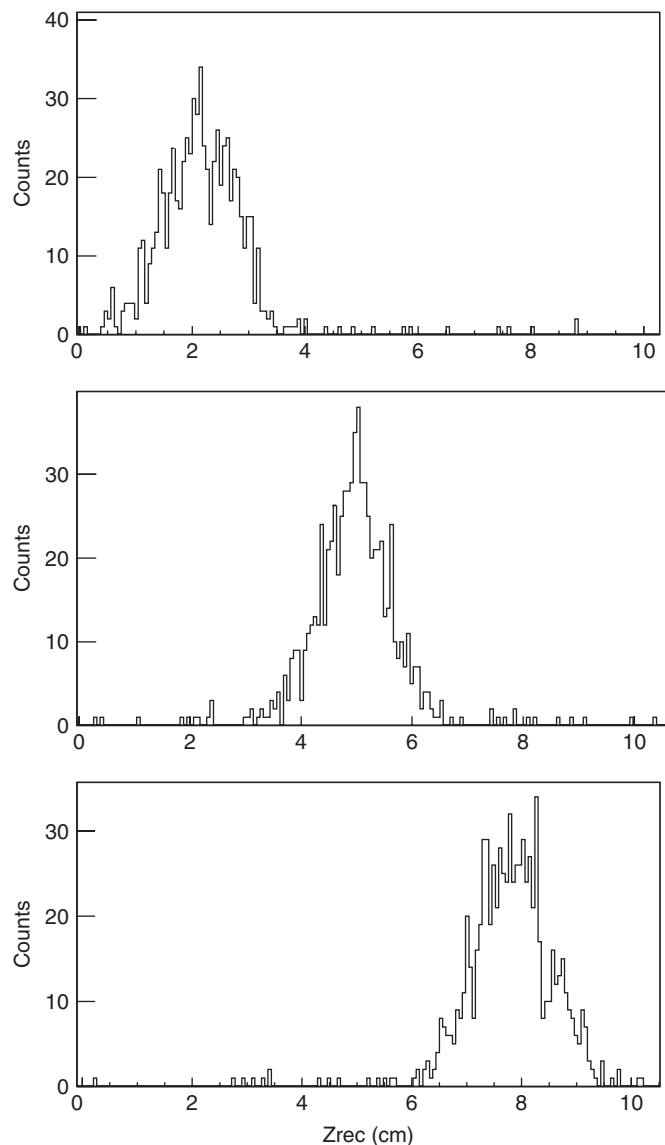
tion. Values of $\sigma_z = 0.8$ and 1.45 cm are found for YAP and LYSO, respectively, essentially constant along the crystal length for polished crystals. The two lower plots show a significantly improved resolution when the crystals are wrapped with Teflon tape: $\sigma_z = 0.6$ and 0.95 cm. However the resolution slightly degrades towards the ends of the crystals. The measured σ_z values in the crystal centre ($z = 5$ cm) are reported in Table 1.

Smaller σ_z values have been reported in Refs. [8,10–12] for shorter LSO crystals. The best resolutions (Δz [FWHM] = 3–4 mm, Refs. [8,10]) have been obtained for 2 cm long crystals with unpolished lateral surfaces, left "as cut by the saw." A worse resolution (Δz [FWHM] = 10 mm) was obtained in Ref. [8] for a polished Teflon-wrapped 2-cm-long LSO crystal.
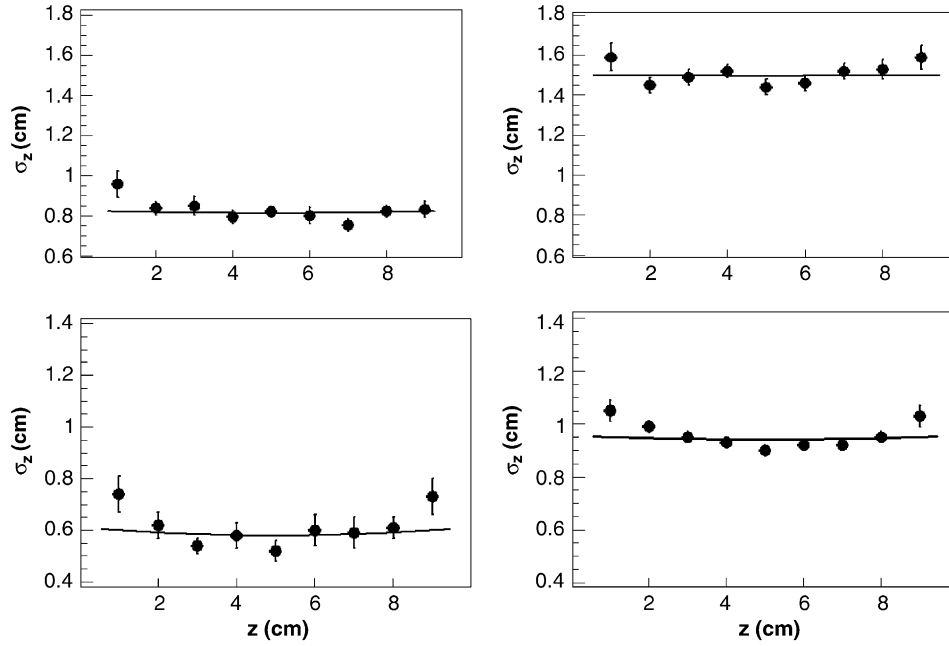
Fig. 10. Uncertainty of *z* reconstruction (standard deviations of the *z*-reconstructed distributions) versus the source *z* position for YAP (left side) and LYSO (right side), polished (top panels) and Teflon-wrapped (bottom panels) crystals. Same abscissa scales in left and right panels, different in top and bottom panels.

The exponential law (Eq. (2)) in determining the axial coordinate *z* (Eq. (1)) provides higher precision than the linear approximation ($z = L_c \times N_1/[N_1 + N_2]$) used in Refs. [8,10–13] and based on the assumption $N_1(z) + N_2(z) = $ const. This assumption is not fulfilled by the exponential trend of all the experimental points shown in Fig. 6.

2.4. Precision of z-reconstruction and energy measurement

To achieve optimum performance both for energy and *z*-reconstruction resolutions, the crystal has to provide high light yield ($\sim N_0$) and adequate short effective light attenuation length (λ_{eff}). These two requirements are to a certain extent contradictory and therefore a good compromise is mandatory. The energy resolution σ_E/E has been derived from the standard deviation of the photopeak of the sum spectra $Q_R + Q_L$, with an ^{22}Na source positioned at the centre of the crystal ($z = 5$ cm). The plots in the upper part of Figs. 11 and 12 show the energy resolution of YAP and LYSO crystals, respectively, as a function of the λ_{eff} values obtained with the different coatings/wrappings. As expected, the energy resolution degrades with decreasing λ_{eff}, while the *z*-resolution, measured at $z = 5$ cm (see the two central panels of Figs. 11 and 12), shows the opposite behaviour, it improves with decreasing λ_{eff}. The resolution in the time difference of the left and right PMT signals, measured at $z = 5$ cm, is displayed in the lower panels. Its behaviour is similar to that of the energy resolution. The interpretation of these plots indicates that the Teflon wrapping provides the best compromise for the tests

performed with 10-cm-long YAP crystals. The experimental resolution values are summarized in Table 1.

To check the internal consistency of our measurements, we derive the number of photoelectrons from the measured energy resolutions. An intrinsic resolution $(\sigma_E/E)_{intr}$ of 1.4% and 5% has been assumed [2,16] for YAP and LYSO, respectively, at 511 keV. The intrinsic resolution is unfolded, and the excess noise factor of the PMT (ENF = 1.4, Ref. [7]) is corrected for:

$$N_{pe}\left(\frac{L_c}{2}\right) = \frac{ENF}{\left(\sigma_E/E\right)^2 - \left(\sigma_E/E\right)^2_{intr.}}, \qquad (5)$$

$$N_0 = N_{pe}\left(\frac{L_c}{2}\right) e^{L_c/2\lambda_{eff}}. \qquad (6)$$

The obtained N_0 values, listed in Table 2, together with the measured values of λ_{eff}, allow us to calculate the expected spatial resolution according to Eq. (1). We multiply the calculated σ_z values by a factor of 1.13 to account for path-length fluctuations [2] which are not included in Eq. (1). The calculated values together with the measured ones are also summarized in Table 2. We find good agreement on the level of 10%, except for 1 nm Cr coating on YAP, where the difference is about 20%. The agreement proves the validity of our approach.

3. Conclusions

This paper is a status report on the various techniques we are exploring for the HPD-PET concept. It deals with
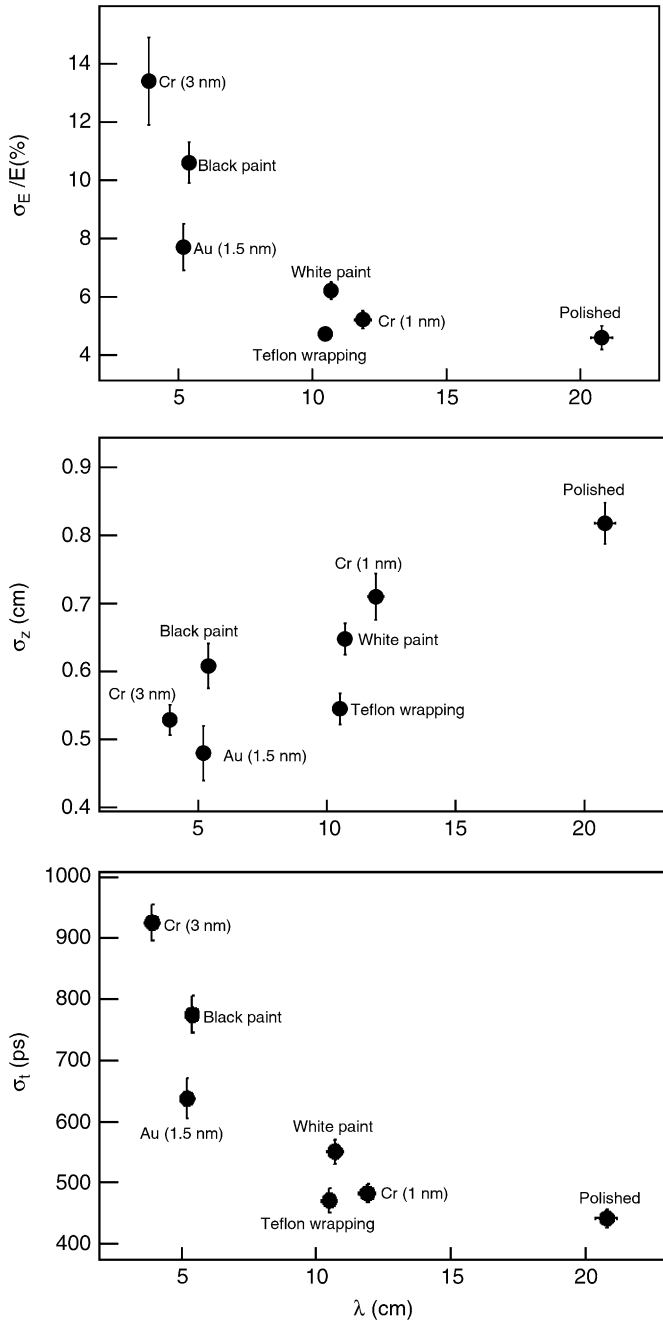
Fig. 11. σ_E/E energy resolutions (top panel), the σ_z position resolutions (central panel) and the σ_t time resolutions (bottom panel) measured with 511 keV γ-rays in the crystal centre ($z = 5$ cm) for YAP crystals at different λ_{eff} values. All the resolutions have been evaluated from the standard deviations of the photopeaks in the sum spectra (left plus right).

Fig. 12. σ_E/E energy resolutions (top panel), the σ_z position resolutions (central panel) and the σ_t time resolutions (bottom panel) measured with 511 keV γ-rays in the crystal centre ($z = 5$ cm) for LYSO crystals at different λ_{eff} values. All the resolutions have been evaluated from the standard deviation of the photopeak in the sum spectra (left plus right).
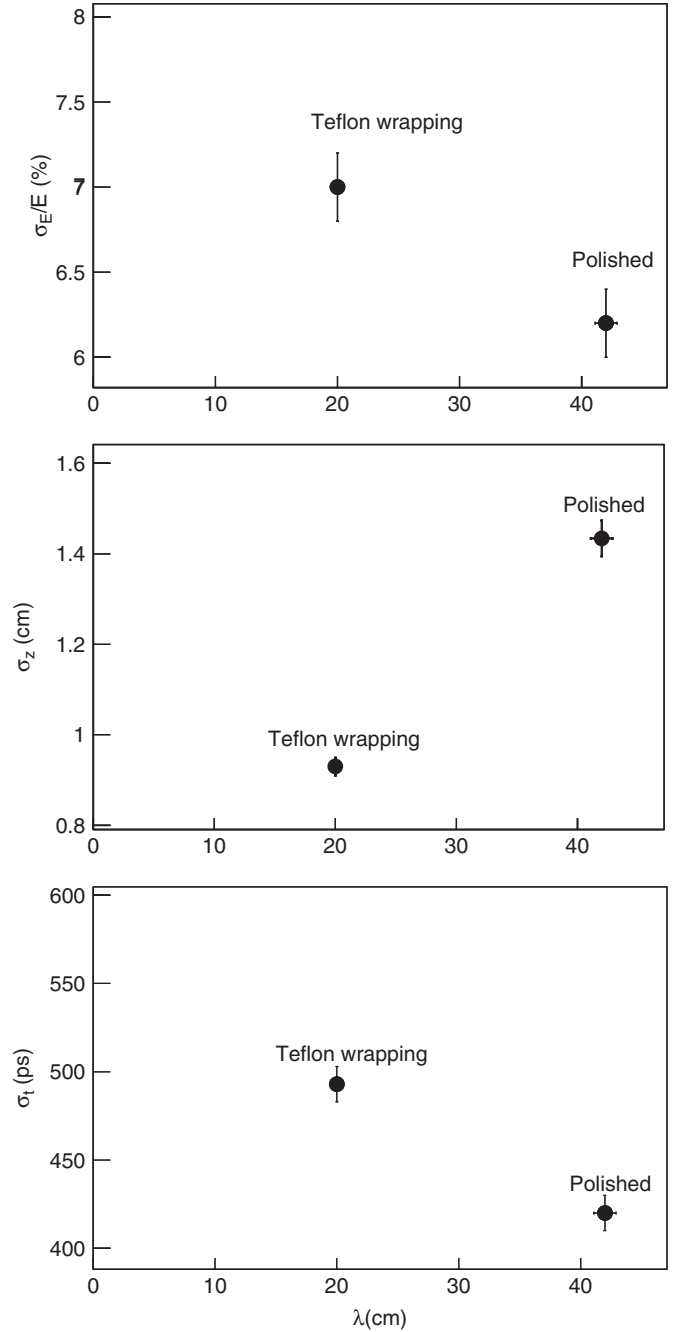
the characterization of 10 cm long polished YAP and LYSO scintillators with 511 keV γ-rays.

The ratio of the N_0 values of polished YAP and LYSO (≈ 1.36 from Fig. 3, (1.26 from Table 2) is in good agreement with the ratio of their light yields quoted in the literature (≈ 1.5). Scans along the crystal bars revealed a fairly good exponential behaviour of the signal with the z coordinate. This behaviour is observed also after wrapping

or coating the crystal lateral surfaces. This allows to reconstruct the z coordinate from the ratio of the signals measured at the two bar ends. This last result validates an important aspect of the 3D axial PET concept.

The examined polished YAP and LYSO crystals were found to be significantly more transparent than those studied in earlier works. The polished LYSO crystals showed a very large effective optical attenuation length of

Table 2
Comparison of expected and measured *z*-resolutions for YAP and LYSO crystals with various coatings for scintillations of 511 keV γ-rays in the centre of the crystal

	λ_{eff} (cm)	σ_E/E (%)	N_0	σ_z (mm) expected	σ_z (mm) measured
YAP polished	20.8	4.6	927	8.7	8.2
YAP Tefl. wrap.	10.5	4.7	1120	4.5	5.4
YAP Cr (1 nm)	11.9	5.2	850	5.65	7.1
YAP Cr (3 nm)	3.9	13.4	284	5.0	5.3
LYSO polished	42.0	6.2	1173	14.7	14.4
LYSO Tefl. wrap.	20.0	7.0	749	9.4	9.3

about 40 cm, i.e. a bulk value of about 50 cm. The polished YAP crystals showed a shorter, but still large, effective attenuation length of about 21 cm, i.e. a bulk value of about 25 cm. Wrapping or coating the crystal lateral surfaces allows decreasing the λ_{eff} value, but also influences N_0. The two parameters affect σ_z, σ_E/E and σ_t. The Teflon wrapping was found to be the best compromise to reduce λ_{eff} and σ_z while maintaining an acceptable N_0 value and hence also good σ_E/E and σ_t resolutions. The Cr coating allows to tune λ_{eff} to the desired value, but it also decreases N_0, and thus is less effective in improving σ_z.

With Teflon wrapping σ_E/E values of 4.7% and 7% have been obtained for YAP and LYSO crystals, respectively. The same wrapping gives σ_z values of 5.4 and 9.3 mm for YAP and LYSO crystals, respectively. The worse LYSO values are most probably caused by a higher intrinsic (non-statistical) term of this scintillator.

Both the YAP and LYSO *z*-resolutions are worse than values obtained in other PET design studies with a read out at both crystal ends performed with raw and short LSO scintillators. We plan to build the 3D axial PET concept with custom-designed HPDs, equipped with a thin sapphire entrance window, which leads to matched refractive indices. For Teflon-wrapped YAP crystals, an improve-

ment of 29% in the σ_z values and of 40% in σ_E/E are expected from simulation codes, which are due to a 50% increase of N_0, a 13% decrease of λ_{eff} and to the ENF value of the HPD very near to 1.

Even if the best resolutions ($\Delta E/E$ (FWHM) = 8%, Δz (FWHM) = 9.8 mm) for the HPD-PET concept are predicted for Teflon-wrapped YAP crystals, the choice of the scintillator wrapping to be used in the final project has not yet been made. Simulation calculations will be performed to extrapolate the presented results to other crystal lengths and to other scintillators. Experimental tests on LaBr$_3$ and LYSO scintillators coupled to HPDs are under preparation. The effect of the variation of the Ce concentration on light yield [17] and optical attenuation length is another approach which we plan to study.

References

[1] The CIMA collaboration, http://www.cima-collaboration.org/.
[2] J. Seguinot, et al., Novel geometrical concept of high performance brain PET scanner—principle, design and performance estimates. CERN preprint PH-EP/2004-050, Nuovo Cimento, in press.
[3] C. Joram, Nucl. Phys. B (Proc. Suppl.) 78 (1999) 407.
[4] A. Braem, et al., Nucl. Instr. and Meth. A 525 (2004) 268.
[5] W.W. Moses, Nucl. Instr. and Meth. A 471 (2001) 209.
[6] G.F. Knoll, Radiation Detection and Measurement, Wiley, New York, p. 344 (ISBN:0-471-07338-5).
[7] C. D'Ambrosio, H. Leutz, Nucl. Instr. and Meth. A 501 (2003) 463.
[8] Y. Shao, et al., IEEE Trans. Nucl. Sci. NS-49 (2002) 649.
[9] F.X. Gentit, The Litrani code, http://gentit.home.cern.ch/gentit/.
[10] P.A. Dokhale, et al., Phys. Med. Biol. 49 (2004) 4293.
[11] J.S. Huber, et al., IEEE Trans. Nucl. Sci. NS-48 (2001) 684;
G.C. Wang, et al., Trans. Nucl. Sci. 51 (2004) 775.
[12] E. Gramsch, et al., IEEE Trans. Nucl. Sci. NS-50 (2003) 307.
[13] W.W. Moses, S.E. Derenzo, IEEE Trans. Nucl. Sci. NS-41 (1994) 1441.
[14] K. Shimizu, et al., IEEE Trans. Nucl. Sci. NS-35 (1988) 717.
[15] http://www.2spi.com/catalog/ltmic/cargille-standard.shtml; http://www.2spi.com/catalog/ltmic/cargille-liquid.html.
[16] A. Del Guerra, et al., IEEE Trans. Nucl. Sci. NS-44 (1997) 2415.
[17] J.A. Mares, et al., Nucl. Instr. and Meth. A 498 (2003) 312.